

Illumination-Adaptive Person Re-identification

Zelong Zeng^{1*} Zhixiang Wang^{2*} Zheng Wang^{3†} Yung-Yu Chuang² Shin’ichi Satoh^{1,3}

¹The University of Tokyo ²National Taiwan University ³National Institute of Informatics

{zzlbz, wangz, satoh}@nii.ac.jp, {r06944046, cyy}@csie.ntu.edu.tw

Abstract

Most person re-identification (ReID) approaches assume that person images are captured under relatively similar illumination conditions. In reality, long-term person retrieval is common and person images are captured under different illumination conditions at different times across a day. In this situation, the performances of existing ReID models often degrade dramatically. This paper addresses the ReID problem with illumination variations and names it as Illumination-Adaptive Person Re-identification (IA-ReID). We propose an Illumination-Identity Disentanglement (IID) network to separate different scales of illuminations apart, while preserving individuals’ identity information. To demonstrate the illumination issue and to evaluate our network, we construct two large-scale simulated datasets with a wide range of illumination variations. Experimental results on the simulated datasets and real-world images demonstrate the effectiveness of the proposed framework.

1. Introduction

Person re-identification (ReID) is a cross-camera retrieval task. Given a query person-of-interest, it aims to retrieve the same person from a database of images collected from multiple cameras [25, 24, 26, 33]. The key challenge of ReID lies in the person’s appearance variations among different cameras. Most previous methods attempt to learn a feature representation that is stable to the appearance variations. They have well investigated how to deal with variations in occlusions [31], resolutions [27], poses [7], etc. However, the influence of ever-changing illumination conditions has been largely ignored. Most popular ReID datasets, such as Market1501 [30] and DukeMTMC-reID [32], have relatively uniform illumination conditions, as their images were captured under similar illumination at the same period of time.

*Co-first Authors

†Corresponding Author

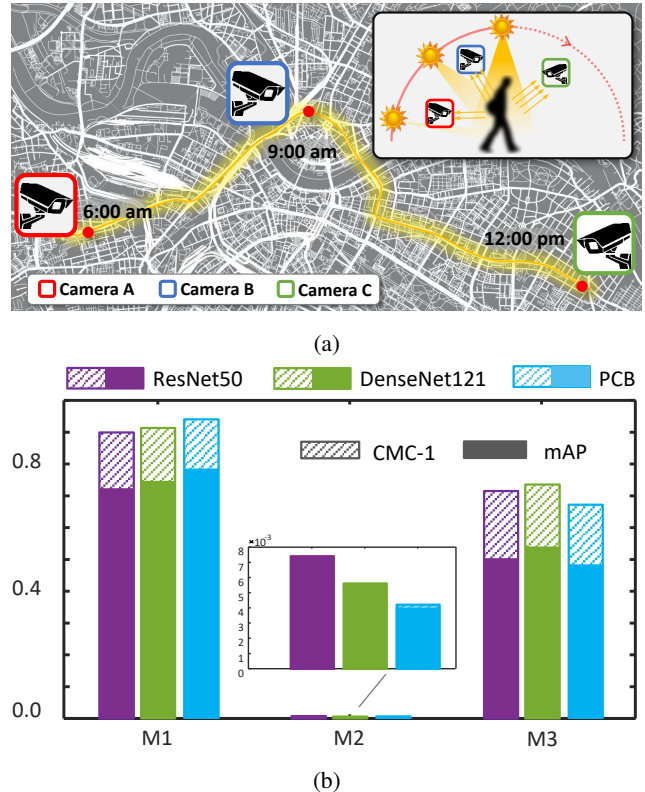


Figure 1: (a) A toy example to illustrate the real application scenario of ReID where images captured at different times could have quite different illumination conditions. (b) The results of preliminary experiments to show the impact of illumination-adaptive. The experiments were conducted on three kinds of networks, including ResNet50 [He *et al.*, 2016], DenseNet121 [Huang *et al.*, 2017], and PCB [Sun *et al.*, 2018]. “M1”, “M2” and “M3” stand for the CMC-1 and mAP results for three different training and testing pairs. “M1” is obtained by training and testing on the Market-1501 dataset. “M2” is obtained by training on the Market-1501++ dataset and testing on the Market-1501++ dataset. “M3” is obtained by training and testing on the Market-1501++ dataset.

In practice, long-term person retrieval is often required in video surveillance networks and criminal investigation applications. As Figure 1(a) shows, the images of a sus-

pect could be taken under very different illumination conditions at different times across a day. He may appear in camera A with dim light at 6:00 a.m., then in camera B with normal light at 9:00 a.m., and finally in camera C with glare light at 12:00 p.m. Existing researches did not investigate this illumination-adaptive issue. We name the ReID task under different illumination conditions as *Illumination-Adaptive Person Re-identification (IA-ReID)*. In this task, given a probe image under one illumination, the goal is to match against gallery images with several different illuminations. The images can be with normal illumination as existing ReID datasets (Market1501, DukeMTMC-reID), can be very bright if captured under dazzling sunshine, and also can be very dark if captured in the sunset or even during the night.

The illumination actually greatly affects the performance of re-identification. As we know, the re-identification performance relies heavily on the characteristics of the datasets. The model trained on one dataset often can not perform well on the other. Traditional models, although efficient and effective to re-identify gallery images with the same illumination, may suffer from a significant performance loss when the illumination conditions of gallery images vary greatly. We have conducted preliminary experiments for demonstrating the performance degradation using the Market-1501 dataset. We simulated different illumination conditions for images in the dataset. The resultant dataset with varying illumination conditions is named the Market-1501++ dataset. Three training-testing configurations were performed: M1 (both train and test on Market-1501), M2 (train on Market-1501 but test on Market-1501++), and M3 (both train and test on Market-1501++). As Figure 1(b) illustrates, 1) the learned models are not stable across datasets with different illuminations (“M2”) and 2) even trained with images under different illumination conditions, the model cannot achieve satisfied performance (“M3”). That is to say, general ReID models lose their effectiveness in the situation with illumination variations.

As far as we know, some researches investigated the issue of different illuminations in ReID [1, 23]. However, they just consider a situation of two scales of illuminations. They assumed that the probe and the gallery images are respectively captured from two cameras, each with a corresponding illumination condition. In such a controlled setting, they proposed to learn the relationship between two scales of illuminations by brightness transfer functions [1] or the feature projection matrix [23]. IA-ReID is a more practical problem with multiple illuminations. Obviously, constructing the relationships among different scales of illuminations is not a practical solution for this problem. If there are 10 different scales in the dataset, the method needs to construct 10 different relationships, and it cannot be guar-

anteed the 10 relationships work perfectly.

Removing the effect of illumination is another intuitive idea. One solution is to do image enhancement [2] for the low-illumination images and image reconstruction [6] for the images with high exposure. However, this kind of methods either cannot handle extreme illuminations [3], or are particularly designed for visualization and rely heavily on the data condition and training samples [2, 6].

Another solution is to disentangle the illumination information apart from the person feature. This idea is learned from the existing face recognition methods [22], where certain face attributes are separated from the feature vector. In this paper, we follow this thread of ideas, and propose an Illumination-Identity Disentanglement (IID) network. Inspired by previous researches dealing with the image resolution issue [27], we construct two simulated illumination-adaptive datasets based on Market1501 [30] and DukeMTMC-reID [32]. Then, these two datasets are utilized to evaluate the effectiveness of IID network. Our contributions can be summarized as follows:

- **A new and practical problem.** We raise a new and practical task, *i.e.*, IA-ReID. The task is practical for long-term person re-identification applications. We construct two simulated datasets with different illuminations to put forward this task. Most general ReID models are proved ineffective when evaluated on these two datasets.
- **A novel method.** We propose a novel Illumination-Identity Disentanglement (IID) network, which separates the illumination information apart from person’s appearance. The method achieves great performance improvement on our two datasets. We also evaluate on some real images, and the network is capable of alleviating the effect of illumination discrepancy.
- **Simple and Effective.** We construct the IID network based on a simple backbone. The network is easy to follow. Extensive experiments prove that IID is robust in long-term person re-identification applications. In this way, we set a benchmark for the new task.

2. Related work

2.1. Short-term ReID

In short-term condition, existing researches paid attention to the challenges from resolution variations [27], pose changes [7] and occlusion [31]. A lot of methods were proposed to learn robust representations to overcome those challenges. They have achieved very high performances on the public datasets. Liao *et al.* [15] analyzed the horizontal occurrence of local features, and maximized the occurrence to make a stable representation against viewpoint changes. Su *et al.* [20] leveraged the human part cues to alleviate

the pose variations and learn robust feature representations from both the global image and different local parts. Zheng *et al.* [31] fused a local patch-level and a global part-based matching model to address the occlusion problem. However, when the re-identification task goes to the long-term situation, the illumination variations come to be the key issue.

Note that we claim that public datasets, such as Market1501 [30] and DukeMTMC-reID [32], have relatively uniform illumination conditions. For both Market1501 and DukeMTMC-reID the file name of each image includes the frame index, which indicates the relative captured time of the corresponding image. The range of frame indexes of all images spans over 90,000 frames for Market1501, i.e., those images were captured in a time span of around one hour (25fps \times 3600s). For DukeMTMC-reID, images were captured in around two hours. It supports our claim that existing ReID datasets were captured in a short period of time and the images have relatively uniform illumination conditions.

2.2. Illumination Problem in ReID

Some researches start to investigate the illumination issue in ReID. [12, 1, 23] consider a situation that the probe and the gallery images respectively captured from two cameras with two different illuminations. Kviatkovsky *et al.* [12] proposed an invariant feature exploiting a structure of color distributions, using different parts of the person. Bhuiyan *et al.* [1] learned robust brightness transfer functions to release the illumination change from one camera to the other. Wang *et al.* [23] designed a feature projection matrix to project image features of one camera to the feature space of another camera. Ma *et al.* [19] just focused on the low illumination problem. They transformed all the images to a uniform low illumination, and proposed a metric learning method to address the low illumination. There are also some researches related to more extreme illumination conditions. They considered that when the imaging condition goes to deep night, the low-illumination image will transform to the infrared image. To this end, [29, 28, 4] paid their attention to the infrared-visible re-identification, where one part of the images are from the visible camera and the other part is from the infrared camera. They designed networks to bridge the gap between infrared and visible images. In this paper, multiple illuminations are taken into consideration, including not only the low illumination images but also the high illumination ones. Our illumination-adaptive setting is more practical for long-term ReID.

2.3. Disentangled Feature Learning

Some previous works tried to disentangle the representations in face tasks, for example pose-invariant recognition [22] and identity-preserving image editing [14]. They

exploited attribute supervision and encoded each attribute as a separate element in the feature vector. Liu *et al.* [16] proposed to learn disentangled but complementary face features with face identification. Disentangled feature learning were investigated in image-to-image translation tasks as well. Lee *et al.* [13] exploited disentangled representation for producing diverse outputs, in particular, a domain-invariant content space capturing shared information across domains and a domain-specific attribute space were proposed. Gonzalez *et al.* [8] introduced the concept of cross-domain disentanglement and separated the internal representation into one shared part and two exclusive parts. There also exists some works using disentangled representations to address the single-image deblurring tasks, such as [18].

As far as we know, there is no work designed to disentangle feature from individuals in ReID. Our method is the first to consider to disentangle the illumination, which is one kind of identity-irrelevant information.

3. Our method

3.1. Overview

Figure 2 depicts the overall architecture of our Illumination-Identity Disentanglement (IID) network. The encoder E takes ResNet-50 as the backbone network and encodes the input image \mathbf{x} into the latent vector $\mathbf{z} = E(\mathbf{x})$, where $\mathbf{z} \in \mathbb{R}^{2048}$. Next, two independent fully-connected (FC) layers, \mathcal{H}_P and \mathcal{H}_I , are employed to project \mathbf{z} into two different feature vectors, the person feature $\mathbf{f}_P = \mathcal{H}_P(\mathbf{z})$ and the identity-irrelevant feature $\mathbf{f}_I = \mathcal{H}_I(\mathbf{z})$. Note that \mathbf{f}_P and \mathbf{f}_I are expected to be respectively stable to illumination variations and irrelevant to person identity. To enforce the disentangled information fully represent the input image, the generator G is used to reconstruct the image $\hat{\mathbf{x}} = G(\mathbf{f}_P, \mathbf{f}_I)$ to approximate the input image \mathbf{x} from the disentangled feature vectors, \mathbf{f}_P and \mathbf{f}_I . The reason why we maintain the disentangled illumination-relevant feature rather than simply getting rid of it is to reduce the potential loss of discriminative information in the identity-relevant feature. Specifically, we use the generator G and feed it with the disentangled identity-relevant and identity-irrelevant features to reconstruct the input with minimum loss of information. If we dump the disentangled illumination-relevant feature without guaranteeing the reconstruction, some useful information could slip away with the removed illumination-relevant feature.

3.2. Disentangled Feature Learning

Identity-relevant feature learning. Given the encoded latent vector \mathbf{z} from the encoder E , the FC layer \mathcal{H}_P projects it to the person feature \mathbf{f}_P , where $\mathbf{f}_P = \mathcal{H}_P(\mathbf{z})$. Since the feature \mathbf{f}_P is required to capture information relevant to per-

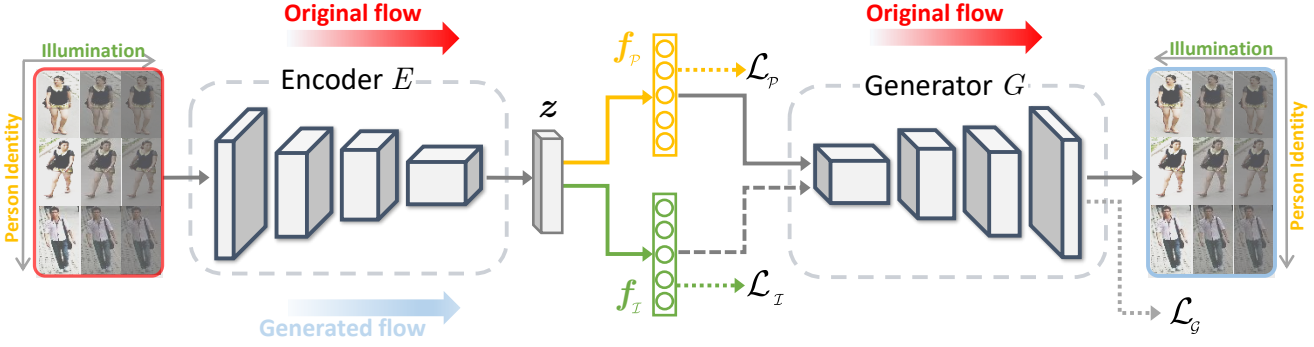


Figure 2: **The architecture of our proposed Illumination-Identity Disentanglement (IID) network.** It consists of an encoder E , a generator G , and two feature embedding layers \mathcal{H}_P and \mathcal{H}_I . The network is optimized through three loss functions. The embedded person (identity-relevant) feature \mathbf{f}_P is trained with the ReID loss \mathcal{L}_P ; the embedded identity-irrelevant feature \mathbf{f}_I is trained with the illumination loss \mathcal{L}_I and the generation loss \mathcal{L}_G is used to guide the optimization of the generator.

son identity, we use the ReID loss \mathcal{L}_P and person identity information to supervise the training process. The ReID loss \mathcal{L}_P combines the triplet loss \mathcal{L}_P^T and the softmax loss \mathcal{L}_P^S and it can be written as

$$\mathcal{L}_P = \lambda_1 \mathcal{L}_P^T + \lambda_2 \mathcal{L}_P^S, \quad (1)$$

where the weights λ_1 and λ_2 are used for balancing these two losses. The training strategy is the same as the one in the general ReID framework; hence the extracted feature can be used for the identification task directly.

The triplet loss is used for similarity learning and it can be formulated as

$$\mathcal{L}_P^T = \sum_{\mathbf{f}_P^a, \mathbf{f}_P^p, \mathbf{f}_P^n \in \mathcal{B}} [\mathcal{D}(\mathbf{f}_P^a, \mathbf{f}_P^p) - \mathcal{D}(\mathbf{f}_P^a, \mathbf{f}_P^n) + \xi]_+, \quad (2)$$

where \mathcal{B} represents a mini-batch consisting of extracted person features \mathbf{f}_P . For an anchor feature vector \mathbf{f}_P^a , the positive sample \mathbf{f}_P^p and the negative sample \mathbf{f}_P^n respectively denotes a feature vector having the same identity with \mathbf{f}_P^a and one with different identity from \mathbf{f}_P^a . Note that $\mathbf{f}_P^a \neq \mathbf{f}_P^p$. ξ is a margin parameter; $\mathcal{D}(\cdot)$ calculates the Euclidean distance; and $[\mathbf{d}]_+ = \max(d, 0)$ truncates negative numbers to zero while keeping positive numbers the same.

The softmax loss is employed for identity information learning, which is written as

$$\mathcal{L}_P^S = -\frac{1}{N} \sum_{j=1}^N \log \hat{y}_P^j, \quad (3)$$

where N is the number of images in the mini-batch \mathcal{B} and \hat{y}_P is the predicted probability of the input belonging to the ground-truth class with $y_P = \text{softmax}(\mathbf{W}_P \mathbf{f}_P + \mathbf{b}_P)$, where \mathbf{W}_P and \mathbf{b}_P are the trainable weight and bias of \mathcal{H}_P respectively.

Identity-irrelevant feature learning. Given the encoded latent vector z from the encoder E , the FC layer \mathcal{H}_I

projects it to the identity-irrelevant feature \mathbf{f}_I , written as $\mathbf{f}_I = \mathcal{H}_I(z)$. To make the feature irrelevant to person identity, we need to feed the network with images taken under different illuminations. Thanks to our simulated dataset, each image is automatically assigned an illumination label, indicating the scale of relative illumination change. Note that the detail information of the datasets is described in Section 4.1. The illumination label is somehow coarse since we made an assumption that images in original datasets are captured in a relatively uniform illumination condition. To eliminate the reliance on this assumption, we make two necessary modifications. 1) We adopt the classifier problem to do regression. 2) We use a soft label strategy instead of the hard label. The soft label strategy is used because we would like to leave some room for tolerating slight changes, possibly caused by camera styles and viewpoints, occurring on this relatively uniform illumination condition. For the same purpose, we also transform the classification problem into a regression problem.

The regression loss is written as

$$\mathcal{L}_I = \frac{1}{N} \sum_{j=1}^N \left\| \hat{c}_I^j - (\mathbf{W}_I \mathbf{f}_I^j + \mathbf{b}_I) \right\|_2^2, \quad (4)$$

where \mathbf{W}_I and \mathbf{b}_I are the trainable weight and bias respectively. The soft label \hat{c}_I is the summation of the ground truth label c_I and Gaussian noise ϵ .

$$\hat{c}_I = c_I + \epsilon, \quad \text{with } \epsilon \in \mathcal{N}(0, 1). \quad (5)$$

Note that there is no difference between the datasets of compared state-of-the-art ReID models and our network. Images with multiple illuminations are just used to separate the illumination information from the person feature.

3.3. Identity-preserving Image Generation

The image generator G is employed to ensure that the disentangled information has minimum information loss. It is fed with the combination of $f_{\mathcal{P}}$ and $f_{\mathcal{I}}$ and generates the reconstructed image $\hat{x} = G(f_{\mathcal{P}}, f_{\mathcal{I}})$. We use the *MSE* loss as the supervision information, which is defined as

$$\mathcal{L}_G = \|\mathbf{x} - \hat{\mathbf{x}}\|_2^2. \quad (6)$$

It is worth mentioning that, in addition to guiding the reconstruction of the input and supervising the training process, G can be used to synthesize images with same identity but varying illuminations by altering the illumination-relevant feature vector $f_{\mathcal{I}}$.

To enforce the reconstructed image \hat{x} identity-preserving, we feed it into the network again. As Figure 2 shows, we name this process as generated flow, instead of original flow. In the generated flow, the loss $\mathcal{L}_{\mathcal{P}}$ and $\mathcal{L}_{\mathcal{I}}$ are taken into account to the total loss function. However, the features $f_{\mathcal{P}}$ and $f_{\mathcal{I}}$ are not needed to utilize again to generate new images.

3.4. Training Process

The training process has three phases: feature disentanglement training, generator training and joint training. Their details will be described as follows.

Phase I: Feature disentanglement training. In this phase, parameters of the disentangled feature learning module are updated. As mentioned above, the disentangled feature learning module consists of the encoder E , two feature embedding layers $\mathcal{H}_{\mathcal{P}}$ and $\mathcal{H}_{\mathcal{I}}$, and the weight and bias $\mathbf{W}_{\mathcal{P}/\mathcal{I}}$, $\mathbf{b}_{\mathcal{P}/\mathcal{I}}$ for loss functions defined in Equation (3) and Equation (4). We denote the parameters of E by θ_E . The parameters of the FC layer $\mathcal{H}_{\mathcal{P}}$, the weights $\mathbf{W}_{\mathcal{P}}$ and the biases $\mathbf{b}_{\mathcal{P}}$ are denoted by $\theta_{\mathcal{P}}$. Similarly, parameters of $\mathcal{H}_{\mathcal{I}}$, $\mathbf{W}_{\mathcal{I}}$ and $\mathbf{b}_{\mathcal{I}}$ are denoted by $\theta_{\mathcal{I}}$. The object function for this phase is

$$\arg \min_{\theta_E, \theta_{\mathcal{P}}, \theta_{\mathcal{I}}} \mathcal{L}_{\mathcal{P}} + \lambda_3 \mathcal{L}_{\mathcal{I}}. \quad (7)$$

We set $\lambda_3 = 1$. Note that $\mathcal{L}_{\mathcal{P}}$ is defined in Equation (1) with the hyperparameters $\lambda_1 = \lambda_2 = 0.5$. The hyperparameter ξ in Equation (2) is set to 0.3.

The encoder E is initialized with ImageNet pretrained weights [5]. Other parts are initialized with He's method [9]. The optimizer utilizes SGD with momentum and weight decay set to 0.9 and 5×10^{-4} . The learning rate for E is set to 0.05 initially and reduced to 0.1 of its previous value every 40 epochs. The learning rate for other parts is 0.1 of the learning rate for E . Algorithm 1 depicts the detailed training procedure of this phase.

Phase II: Generator training. With the disentangled feature learning modules $\{E, \mathcal{H}_{\mathcal{P}/\mathcal{I}}, \mathbf{W}_{\mathcal{P}/\mathcal{I}}, \mathbf{b}_{\mathcal{P}/\mathcal{I}}\}$ fixed, we optimize the image generator G with the Adam optimizer in

Algorithm 1: Phase I of the training procedure.

Input: Training data $\{\mathbf{x}_i\}$ along with the identity label $c_{\mathcal{P}}^i$ and the illumination label $c_{\mathcal{I}}^i$.
 Initialized parameters $\theta_{\mathcal{P}}$ and $\theta_{\mathcal{I}}$.
 Hyperparameters $\lambda_{1,2,3}$, ξ and learning rate μ^t .
 The number of iterations $t \leftarrow 0$.

Output: Parameters θ_E , $\theta_{\mathcal{P}}$ and $\theta_{\mathcal{I}}$.

```

1 while not converge do
2    $t \leftarrow t + 1$ .
3   Compute the joint loss by  $\mathcal{L}^t = \mathcal{L}_{\mathcal{P}}^t + \lambda_3 \mathcal{L}_{\mathcal{I}}^t$ .
4   Compute the back-propagation error  $\frac{\partial \mathcal{L}^t}{\partial \mathbf{x}_i^t}$  for each
    $i$  by  $\frac{\partial \mathcal{L}^t}{\partial \mathbf{x}_i^t} = \frac{\partial \mathcal{L}_{\mathcal{P}}^t}{\partial \mathbf{x}_i^t} + \lambda_3 \frac{\partial \mathcal{L}_{\mathcal{I}}^t}{\partial \mathbf{x}_i^t}$ .
5   Update the parameters  $\theta_E$ ,  $\theta_{\mathcal{P}}$  and  $\theta_{\mathcal{I}}$ 
6 end

```

phase II. The learning rate is set to 0.01 and reduced to 0.1 of its previous value every 40 epochs. Our task is to reconstruct the input images, *i.e.*, minimize the *MSE* loss. The objective function is

$$\arg \min_{\theta_G} \mathcal{L}_G, \quad (8)$$

where θ_G represents parameters of the generator G .

Phase III: Joint training. Finally, we jointly train the entire network in an end-to-end manner and the overall objective function is expressed as

$$\arg \min_{\theta_E, \theta_{\mathcal{P}}, \theta_{\mathcal{I}}, \theta_G} \mathcal{L}_{\mathcal{P}} + \lambda_3 \mathcal{L}_{\mathcal{I}} + \lambda_4 \mathcal{L}_G. \quad (9)$$

We use Adam optimizer for optimizing the overall objective function. The initial learning rate for the feature disentanglement part and the generator part is set to 1×10^{-4} and 1×10^{-3} respectively. It decreases to 0.1 of its previous value every 50 epochs. The hyperparameters are $\lambda_3 = 1$ and $\lambda_4 = 2$. The generation process gifts the network more ability of disentangling illumination feature. Hence, a joint learning manner will better balance the network's abilities of re-identification and disentanglement.

4. Experiments

4.1. Experimental Settings

Datasets. There are two widely used datasets under normal illumination, *i.e.*, Market-1501 [30] and DukeMTMC-reID [32]. For Market-1501, it consists of 12,936 images of 751 identities for training and 19,281 images of 750 identities in the gallery set for testing. For DukeMTMC-reID, it contains 16,522 training images with 702 identities, 2,228 query images of the other 702 identities and 17,661 gallery images.



(a) Market-1501++



(b) DukeMTMC-reID++

Figure 3: **Sample images of two simulated datasets.** Each row shows images of the same identity. For each identity, the images have different illuminations. (a) The Market-1501++ dataset. (b) The DukeMTMC-reID++ dataset.

Based on these two datasets, we constructed two simulated illumination-adaptive datasets. Considering that a slight illumination variation does not change the representation too much, and also that multiple scales of illuminations are required to simulate a wide-range of illumination variation, we selected nine scales of illuminations. We adapt each image to random one of nine illuminations. We apply a random gamma adjustment to each channel of the common images to produce the illumination-adaptive images, which is similar to [17]. The recorded value of an image captured by a camera is usually nonlinearly mapped from its corresponding scene radiance, and the nonlinearity often can be well approximated by a power function. The variance in the real-world illumination is then nonlinearly related to the image intensity. Therefore, we applied the nonlinear gamma transform to the decomposed illumination for simulating images under different illumination conditions. To make the illumination change reasonable, we further add Poisson noise with peak value = 10 to illumination changed images. Finally, we constructed the simulated illumination-adaptive datasets and named them as Market-1501++ and DukeMTMC-reID++. We consider that gamma transform is insufficient to model non-global illumination variation. However, although local illumination variation could affect face identification significantly, person ReID relies mostly on global information and is consequently less sensitive to local illumination variation. Thus, we only consider the global illumination variation.

Evaluation metrics. To indicate the performance, the stan-

dard Cumulative Matching Characteristics (CMC) values and mean Average Precision (mAP) are adopted [30], since one person has multiple ground truths in the gallery set.

Real-world images. To prove the effectiveness of the proposed method on reducing the effect of illuminations, we also collected some real-world images with different illuminations. Note that we collected real-world image indoors. Because of the controllable indoor environment, we can collect diverse real-world images easily. We will collect more real-world images outdoors (at morning, noon and night-fall) in the future. Through calculating the distances, we show the ability of the proposed IID network. Some examples are shown in Figure 5.

We made an illumination analysis of related datasets. We used the average value of the pixel luminance of each image to represent its illumination. We investigated the illumination of Market-1501 and DukeMTMC-reID datasets by the illumination distribution. We also made a comparison of the variance of the image illumination on related datasets. Figure 4 shows the results. We can find that the illumination variances of the simulated datasets and the real dataset are extremely larger than that of the existing ReID datasets. Hence, existing ReID datasets were captured in a short period of time and the images have relatively uniform illumination conditions. We introduce a person re-identification task in an illumination-adaptive condition.

Table 1: Comparison with the state-of-the-art methods on the Market-1501++ and DukeMTMC-reID++ datasets. CMC-1, CMC-5, CMC-10 (%) and mAP (%) are reported.

Method	Market-1501++				DukeMTMC-reID++			
	CMC-1	CMC-5	CMC-10	mAP	CMC-1	CMC-5	CMC-10	mAP
DenseNet121 [11]	0.74	2.29	3.53	0.73	1.21	2.74	4.13	0.80
DenseNet121 w/ Train	70.60	85.36	89.66	49.79	64.45	77.82	82.45	45.12
PCB [21]	0.56	1.69	2.91	0.54	0.72	2.15	3.23	0.49
PCB w/ Train	72.55	85.22	90.08	53.11	65.98	77.93	82.21	45.15
ResNet50 [10]	0.42	1.16	2.05	0.39	0.54	1.97	3.14	0.50
ResNet50 w/ Train (Baseline)	66.18	81.97	87.02	47.71	62.07	75.54	88.08	42.63
IID	73.37	86.55	91.01	56.22	68.11	79.75	91.27	49.20
Improvement over baseline	7.19↑	4.58↑	3.99↑	8.51↑	6.04↑	4.21↑	3.19↑	6.57↑

Table 2: Ablation study on the Market1501++ dataset. CMC-1 (%) and mAP (%) are reported.

Method	Components				Market-1501++	
	\mathcal{L}_P^T	\mathcal{L}_P^S	\mathcal{L}_I	\mathcal{L}_G	CMC-1	mAP
Baseline	✓	✓	✗	✗	66.18	47.71
IID (no G)	✓	✓	✓	✗	71.54	55.17
IID (no triplet for id)	✗	✓	✓	✓	64.14	45.87
IID (no softmax for id)	✓	✗	✓	✓	65.21	46.53
IID (no illum.)	✓	✓	✗	✓	70.79	54.57
IID	✓	✓	✓	✓	73.37	56.22

4.2. Comparison with State-of-The-Arts

In this subsection, we make comparisons with the state-of-the-art methods. We exploit the Market-1501++ and the DukeMTMC-reID++ datasets to evaluate the methods. As IA-ReID is new, there are barely methods for comparisons. We selected DenseNet121 [11], PCB [21] and ResNet50 [10] as the comparison methods. DenseNet121 and ResNet50 are two popular baseline networks in ReID. PCB is one of the state-of-the-art ReID methods. Table 1 list their results. Note that the notation with a ‘w/ Train’ suffix means that the indicated model has been trained on the illumination-adaptive datasets before testing. From the table, we can find that the results of DenseNet121, PCB and ResNet50 drop dramatically when facing the IA-ReID dataset. However, all of these three deep networks can obtain relative high promotions when training on the illumination-adaptive data, which means that the deep learning network can somehow deal with part of the illumination-adaptive issue.

We took ResNet50 as our baseline. From the table, we can find that, compare with the baseline (serving it as our backbone network), our method improves the performance on both of the simulated Market-1501++ and DukeMTMC-reID++ datasets. Thus, The improvement against the baseline better shows the effectiveness of the proposed method

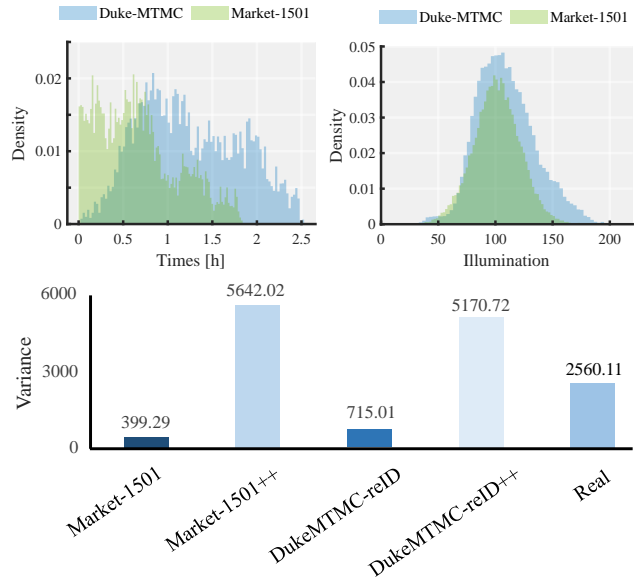


Figure 4: **Illumination analysis of related datasets.** We used the average value of the pixel luminance of each image to represent its illumination. The top two figures show the illumination distributions of Market-1501 and DukeMTMC-reID datasets. We can find that images are randomly captured around one and two hours respectively, and their illuminations are not changing too much with the mean value 100. The bottom figure shows the variance of the image illumination on related datasets. We can find that the illumination variances of the simulated datasets (Market-1501++, DukeMTMC-reID++) and the real dataset are larger than that of the existing ReID datasets (Market-1501, DukeMTMC-reID).

as they share the same backbone architecture. Although we do not report improvements against other methods, from Table 1, it is clear that our method outperforms all methods.



Figure 5: **Sample images of the collected real-world images.** Each row shows images of one identity.

Table 3: Comparison with the baseline on the Market-1501 and DukeMTMC-reID datasets. CMC-1 (%) and mAP (%) are reported.

Method	Market-1501		DukeMTMC-reID	
	CMC-1	mAP	CMC-1	mAP
Baseline	88.84	71.49	79.71	61.77
IID	88.45	71.46	78.10	60.56

4.3. Ablation Study

Our method consists of four kinds of losses. The triplet loss \mathcal{L}_P^T and the cross-entropy loss \mathcal{L}_P^S are responsible for extracting robust person features. The regression loss \mathcal{L}_I is responsible for predicting accurate illumination features. The MSE loss \mathcal{L}_G is used for image reconstruction. Removing either of them affects re-identification or illumination disentanglement that influences re-identification indirectly. Thus it degrades the performance.

Here, we take the Market-1501++ dataset as an exam-

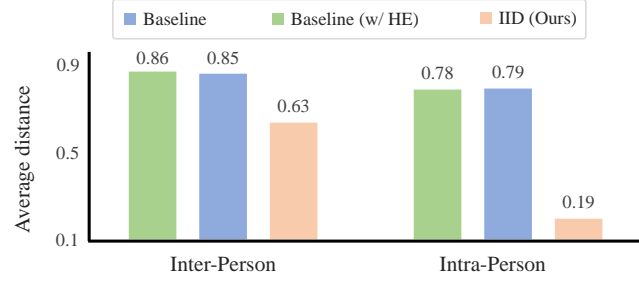


Figure 6: **The average values of intra-person distances and inter-person distance for real-world images.** The experiments are respectively conducted by the baseline method, baseline method fed with image after histogram equalization (w/ HE) and our IID method.

ple to do the ablation study. When removing both of \mathcal{L}_I and \mathcal{L}_G (the baseline), the performance drops to 66.18% CMC-1 and 47.71% mAP, as it can only rely on the person feature without separating the illumination feature. When removing \mathcal{L}_G , the performance does not drop so much as the baseline. The loss \mathcal{L}_I is useful for separating the illumination information and promotes the re-identification result. When removing \mathcal{L}_P^T or \mathcal{L}_P^S , the performance drops dramatically even worse than the baseline. So the loss for re-identification is still important for the IA-ReID task. When removing \mathcal{L}_I , the performance does not drop so much as the baseline. So even without the loss for illumination regression, the generation process can also benefit the illumination disentanglement.

4.4. Experiments on General ReID Datasets

Although we design a new network for the IA-ReID task, we do not expect the proposed IID network perform poorly on the general ReID dataset. As our network is proposed based on the baseline network Resnet50, we make a comparison with the baseline. The results are list in Table 3. From the table, we can find that the results do not change too much. Although the IID network is specially designed for the illumination-adaptive condition, it is still suitable for the general ReID task.

4.5. Experiments on Illumination Prediction

As we know, the disentangled illumination feature can be used to predict the illumination scale of each image. We test its prediction accuracy on the Market-1501++ and DukeMTMC-reID++ datasets. The results are very high, which are 98.74% and 98.53% respectively for the Market-1501++ and DukeMTMC-reID++ datasets. It means that the disentangled illumination feature can well represent the illumination scale.

4.6. Experiments on the Real-world Images

We recruited 15 volunteers and for each volunteer we collected 10 images under different illumination conditions. Some examples are shown in Figure 5. We calculated the intra-person distances and inter-person distances respectively with the baseline model, the baseline model with histogram equalization, and the proposed IID network. We recorded the average values of the intra-person distances and inter-person distances. Figure 6 shows the final results. We can find that the proposed IID is more effective to reduce the intra-person distance, *i.e.*, to alleviate the effect of the illumination change.

5. Conclusion

This paper raises a new issue, which has not been investigated before as far as we know. Traditional models under multi-illuminations may not be proper for this task. We propose to disentangle the illumination feature apart to address the new problem. Experimental results illustrate that the traditional model has a significant loss of performance when the illumination of gallery images are different and the scales vary unsteadily, and demonstrate the effectiveness of the proposed network.

Disentangled representation learning is an effective mechanism to distill significant information from the mixed feature representation. As far as we know, we are the first to explore this mechanism to the theme of person ReID, especially to the novel long-term person ReID problem. Compared with the work in the field of face identification, the proposed model further predicts the scale of the illumination and strengthens the re-identification ability of identity features. By showing its effectiveness, we hope the method can also help address problems in other application domains. In addition, our main contribution lies in pointing out an important problem for long-term person ReID and demonstrating promising initial results. We believe that our paper could inspire more work along this direction and make the ReID techniques more practical.

References

[1] Amran Bhuiyan, Alessandro Perina, and Vittorio Murino. Exploiting multiple detections to learn robust brightness transfer functions in re-identification systems. In *IEEE International Conference on Image Processing*, pages 2329–2333, 2015. 2, 3

[2] Chen Chen, Qifeng Chen, Jia Xu, and Vladlen Koltun. Learning to see in the dark. In *Proceedings of the IEEE Conference on Computer Vision and Pattern Recognition*, 2018. 2

[3] Yu-Sheng Chen, Yu-Ching Wang, Man-Hsin Kao, and Yung-Yu Chuang. Deep photo enhancer: Unpaired learning for image enhancement from photographs with gans. In *Proceedings of the IEEE Conference on Computer Vision and Pattern Recognition*, 2018. 2

[4] Pingyang Dai, Rongrong Ji, Haibin Wang, Qiong Wu, and Yuyu Huang. Cross-modality person re-identification with generative adversarial training. In *Proceedings of the International Joint Conferences on Artificial Intelligence*, pages 677–683, 2018. 3

[5] Jia Deng, Wei Dong, Richard Socher, Li-Jia Li, Kai Li, and Li Fei-Fei. Imagenet: A large-scale hierarchical image database. In *Proceedings of the IEEE Conference on Computer Vision and Pattern Recognition*, pages 248–255, 2009. 5

[6] Gabriel Eilertsen, Joel Kronander, Gyorgy Denes, Rafał K Mantiuk, and Jonas Unger. Hdr image reconstruction from a single exposure using deep cnns. *ACM Trans. Graphics*, 2017. 2

[7] Yixiao Ge, Zhuowan Li, Haiyu Zhao, Guojun Yin, Shuai Yi, Xiaogang Wang, et al. FD-GAN: Pose-guided feature distilling gan for robust person re-identification. In *Proceedings of the Advances in Neural Information Processing Systems*, pages 1222–1233, 2018. 1, 2

[8] Abel Gonzalez-Garcia, Joost van de Weijer, and Yoshua Bengio. Image-to-image translation for cross-domain disentanglement. In *Proceedings of the Advances in Neural Information Processing Systems*, pages 1287–1298, 2018. 3

[9] Kaiming He, Xiangyu Zhang, Shaoqing Ren, and Jian Sun. Delving deep into rectifiers: Surpassing human-level performance on imagenet classification. In *Proceedings of the IEEE International Conference on Computer Vision*, pages 1026–1034, 2015. 5

[10] Kaiming He, Xiangyu Zhang, Shaoqing Ren, and Jian Sun. Deep residual learning for image recognition. In *Proceedings of the IEEE Conference on Computer Vision and Pattern Recognition*, pages 770–778, 2016. 7

[11] Gao Huang, Zhuang Liu, Laurens Van Der Maaten, and Kilian Q Weinberger. Densely connected convolutional networks. In *Proceedings of the IEEE Conference on Computer Vision and Pattern Recognition*, 2017. 7

[12] Igor Kviatkovsky, Amit Adam, and Ehud Rivlin. Color invariants for person reidentification. *IEEE Transactions on Pattern Analysis and Machine Intelligence*, 35(7):1622–1634, 2013. 3

[13] Hsin-Ying Lee, Hung-Yu Tseng, Jia-Bin Huang, Maneesh Singh, and Ming-Hsuan Yang. Diverse image-to-image translation via disentangled representations. In *Proceedings of the European Conference on Computer Vision*, pages 35–51, 2018. 3

[14] Mu Li, Wangmeng Zuo, and David Zhang. Deep identity-aware transfer of facial attributes. *arXiv preprint arXiv:1610.05586*, 2016. 3

[15] Shengcai Liao, Yang Hu, Xiangyu Zhu, and Stan Z Li. Person re-identification by local maximal occurrence representation and metric learning. In *Proceedings of the IEEE Conference on Computer Vision and Pattern Recognition*, pages 2197–2206, 2015. 2

[16] Yu Liu, Fangyin Wei, Jing Shao, Lu Sheng, Junjie Yan, and Xiaogang Wang. Exploring disentangled feature representation beyond face identification. In *Proceedings of the IEEE Conference on Computer Vision and Pattern Recognition*, 2018. 2

Conference on Computer Vision and Pattern Recognition, pages 2080–2089, 2018. 3

[17] Kin Gwn Lore, Adedotun Akintayo, and Soumik Sarkar. Llnet: A deep autoencoder approach to natural low-light image enhancement. *Pattern Recognition*, 2017. 6

[18] Boyu Lu, Jun-Cheng Chen, and Rama Chellappa. Unsupervised domain-specific deblurring via disentangled representations. *arXiv preprint arXiv:1903.01594*, 2019. 3

[19] Fei Ma, Xiaoke Zhu, Xinyu Zhang, Liang Yang, Mei Zuo, and Xiao-Yuan Jing. Low illumination person re-identification. *Multimedia Tools and Applications*, 78(1):337–362, 2019. 3

[20] Chi Su, Jianing Li, Shiliang Zhang, Junliang Xing, Wen Gao, and Qi Tian. Pose-driven deep convolutional model for person re-identification. In *Proceedings of the IEEE International Conference on Computer Vision*, pages 3960–3969, 2017. 2

[21] Yifan Sun, Liang Zheng, Yi Yang, Qi Tian, and Shengjin Wang. Beyond part models: Person retrieval with refined part pooling (and a strong convolutional baseline). In *Proceedings of the European Conference on Computer Vision*, pages 480–496, 2018. 7

[22] Luan Tran, Xi Yin, and Xiaoming Liu. Disentangled representation learning gan for pose-invariant face recognition. In *Proceedings of the IEEE Conference on Computer Vision and Pattern Recognition*, pages 1415–1424, 2017. 2, 3

[23] Yimin Wang, Ruimin Hu, Chao Liang, Chunjie Zhang, and Qingming Leng. Camera compensation using a feature projection matrix for person reidentification. *IEEE Transactions on Circuits and Systems for Video Technology*, 24(8):1350–1361, 2014. 2, 3

[24] Zheng Wang, Ruimin Hu, Chen Chen, Yi Yu, Junjun Jiang, Chao Liang, and Shin’ichi Satoh. Person reidentification via discrepancy matrix and matrix metric. *IEEE Transactions on Cybernetics*, 48(10):3006–3020, 2018. 1

[25] Zheng Wang, Ruimin Hu, Chao Liang, Yi Yu, Junjun Jiang, Mang Ye, Jun Chen, and Qingming Leng. Zero-shot person re-identification via cross-view consistency. *IEEE Transactions on Multimedia*, 18(2):260–272, 2016. 1

[26] Zheng Wang, Junjun Jiang, Yi Yu, and Shin’ichi Satoh. Incremental re-identification by cross-direction and cross-ranking adaption. *IEEE Transactions on Multimedia*, 2019. 1

[27] Zheng Wang, Mang Ye, Fan Yang, Xiang Bai, and Shin’ichi Satoh. Cascaded SR-GAN for scale-adaptive low resolution person re-identification. In *Proceedings of the International Joint Conferences on Artificial Intelligence*, pages 3891–3897, 2018. 1, 2

[28] Ancong Wu, Wei-Shi Zheng, Hong-Xing Yu, Shaogang Gong, and Jianhuang Lai. Rgb-infrared cross-modality person re-identification. In *Proceedings of the IEEE International Conference on Computer Vision*, pages 5380–5389, 2017. 3

[29] Mang Ye, Zheng Wang, Xiangyuan Lan, and Pong C. Yuen. Visible thermal person re-identification via dual-constrained top-ranking. In *Proceedings of the International Joint Conferences on Artificial Intelligence*, pages 1092–1099, 2018. 3

[30] Liang Zheng, Liyue Shen, Lu Tian, Shengjin Wang, Jing-dong Wang, and Qi Tian. Scalable person re-identification: A benchmark. In *Proceedings of the IEEE International Conference on Computer Vision*, pages 1116–1124, 2015. 1, 2, 3, 5, 6

[31] Wei-Shi Zheng, Xiang Li, Tao Xiang, Shengcai Liao, Jianhuang Lai, and Shaogang Gong. Partial person re-identification. In *Proceedings of the IEEE International Conference on Computer Vision*, pages 4678–4686, 2015. 1, 2, 3

[32] Zhedong Zheng, Liang Zheng, and Yi Yang. Unlabeled samples generated by gan improve the person re-identification baseline in vitro. In *Proceedings of the IEEE International Conference on Computer Vision*, pages 3754–3762, 2017. 1, 2, 3, 5

[33] Zhun Zhong, Liang Zheng, Zhedong Zheng, Shaozi Li, and Yi Yang. Camera style adaptation for person re-identification. In *Proceedings of the IEEE Conference on Computer Vision and Pattern Recognition*, pages 5157–5166, 2018. 1